

Supporting Information

Intrinsically Robust Cubic MnCoO_x Solid Solution: Achieving High Activity for Sustainable Acidic Water Oxidation

Jingjing Zhang,^{a,b†} Ali Raza,^{c†} Yang Zhao,^{a†} Song Guo,^{a*} Zaheer Ud Din Babar,^{c,d} Liangliang Xu,^{f*}
Changhai Cao,^{ae} and Gao Li^{a,b*}

^a State Key Laboratory of Catalysis, Dalian Institute of Chemical Physics, Chinese Academy of Sciences, Dalian 116023, Liaoning, China

^b University of Chinese Academy of Sciences, Beijing, China

^c Department of Physics “Ettore Pancini”, University of Naples Federico II, Piazzale Tecchio, 80, 80125 Naples, Italy

^d Scuola Superiore Meridionale (SSM), University of Naples Federico II, Largo S. Marcellino, 10, 80138, Italy

^e Key Laboratory of Biofuels and Biochemical Engineering, SINOPEC Dalian Research Institute of Petroleum and Petrochemicals Co., Ltd, Dalian 116045, China

^f Department of Chemical and Biomolecular Engineering, Korea Advanced Institute of Science and Technology (KAIST), 291 Daehak-Ro, Yuseong-Gu, Daejeon 34141, Republic of Korea

†These authors contribute equally in this work.

*Corresponding authors. E-mail addresses: soong_guo@dicp.ac.cn (S. Guo), xuliang@kaist.ac.kr (L. Xu), gaoli@dicp.ac.cn (G. Li)

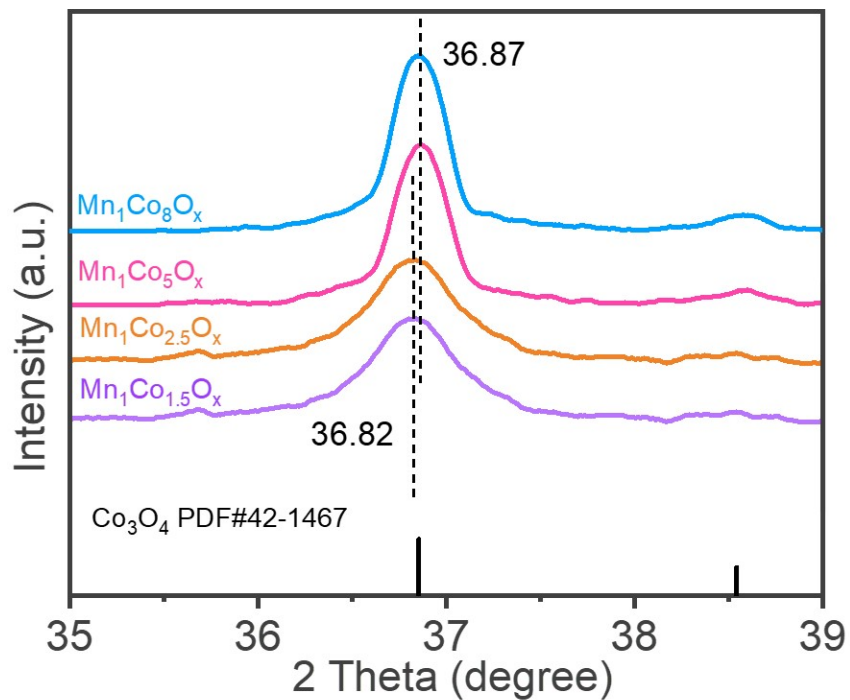


Fig. S1 Zoom-in of XRD patterns of the MnCoO_x catalyst from Figure 1b.

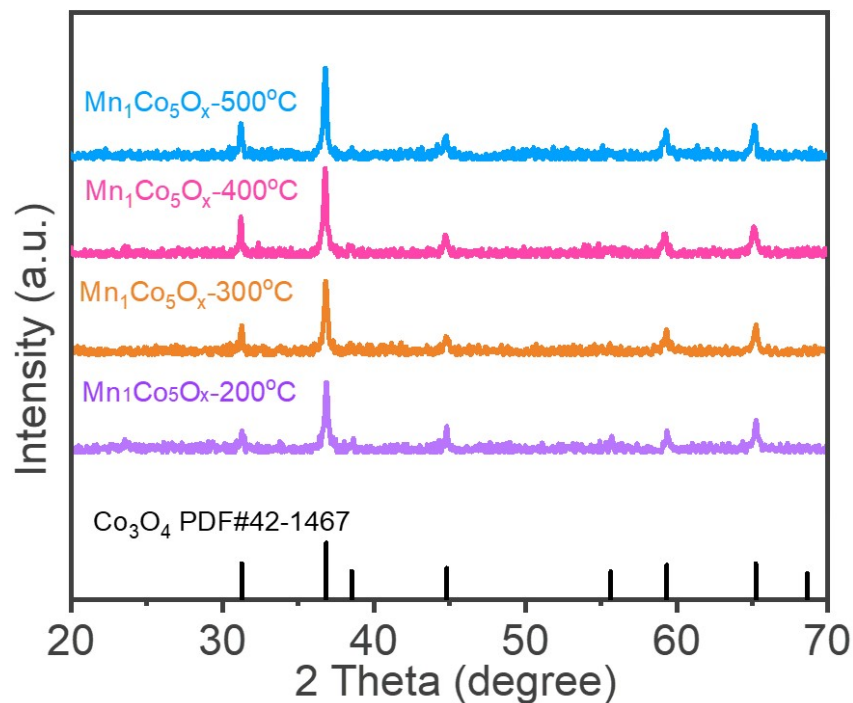


Fig. S2 XRD patterns of the $\text{Mn}_1\text{Co}_5\text{O}_x$ catalyst annealed at different temperatures.

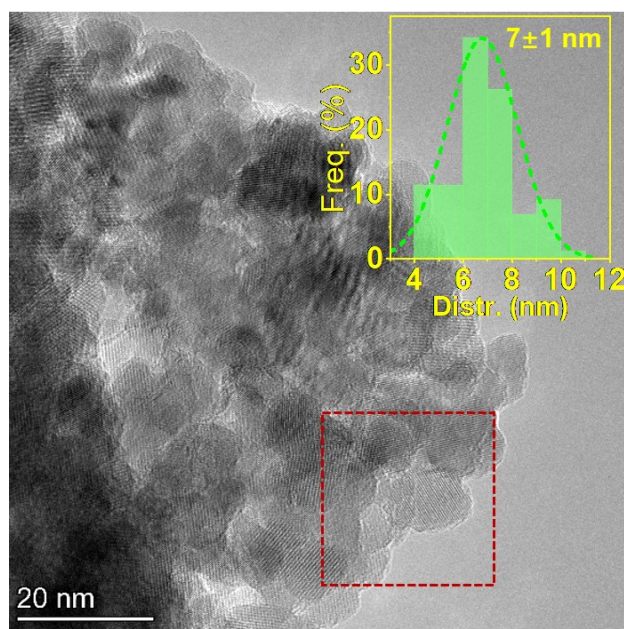


Fig. S3 TEM image of Mn₁Co₅O_x catalyst and the inserted picture shows the size distribution.

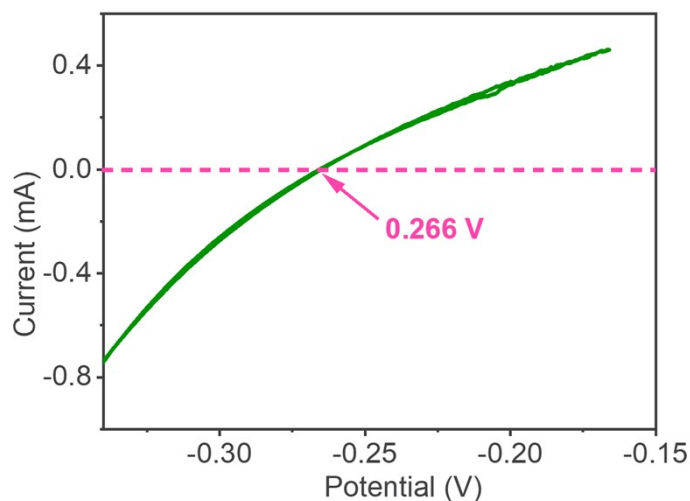


Fig. S4 The calibration CV curve with the scan rate of 1 mV/s for the reference electrode (Hg/Hg₂Cl₂) in a 0.5 M H₂SO₄ (pH 0) solution at room temperature.

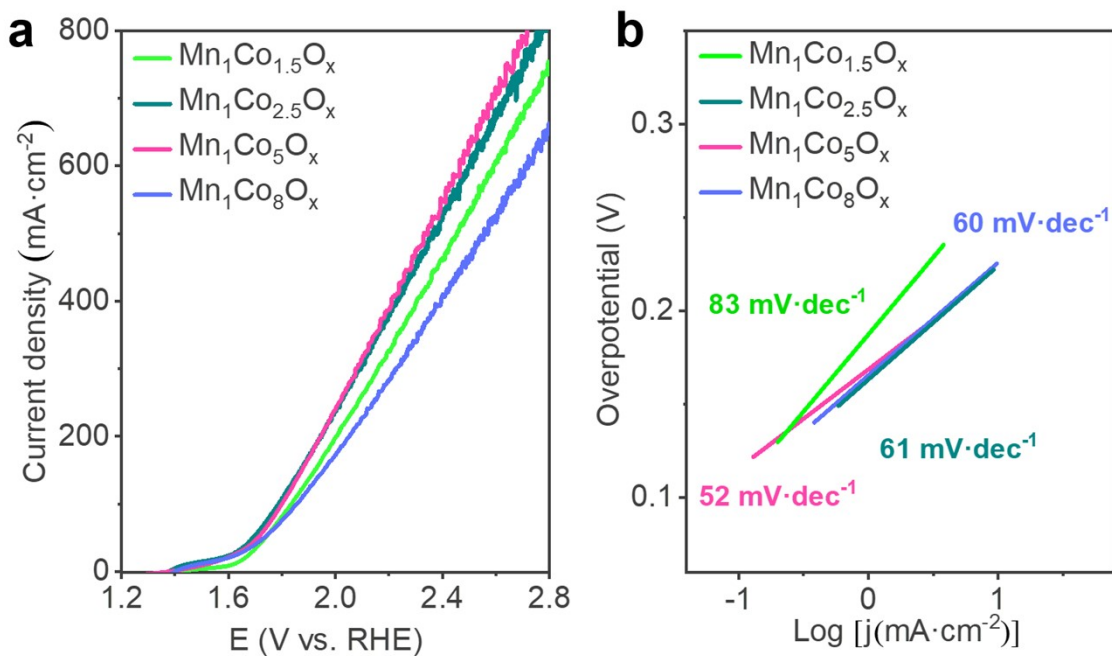


Fig. S5 OER polarization curves and corresponding Tafel slopes of MnCo_yO_x ($y=1.5, 2.5, 5$, and 8) nanocomposites in a $0.5 \text{ M H}_2\text{SO}_4$ (pH 0) solution at room temperature.

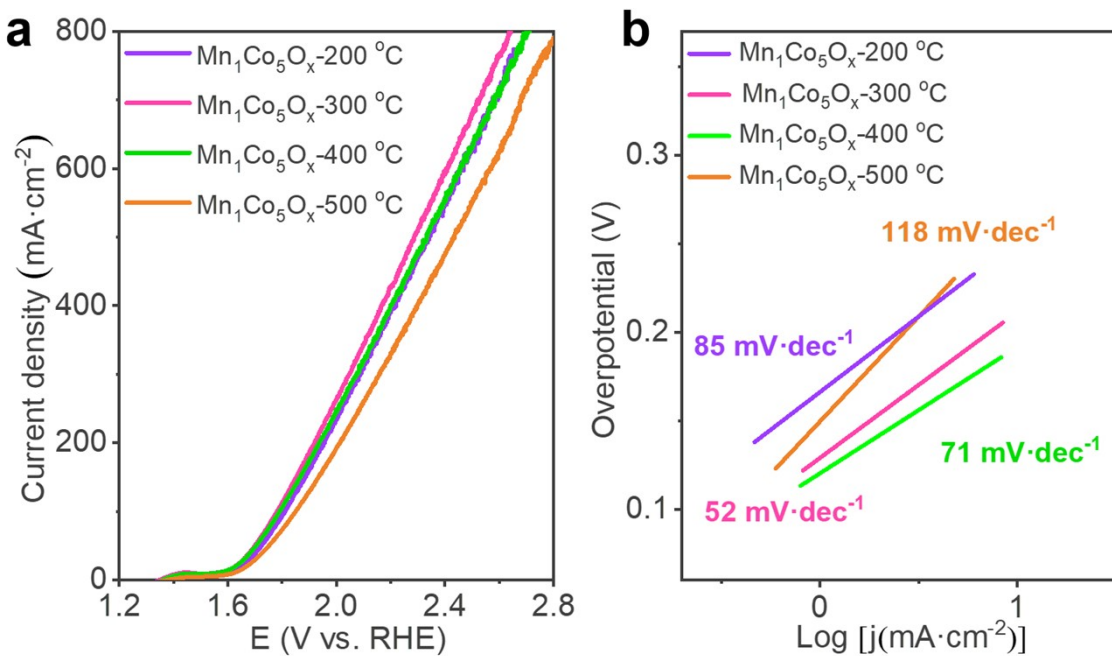


Fig. S6 OER polarization curves and corresponding Tafel slopes of $\text{Mn}_1\text{Co}_5\text{O}_x$ nanocomposites annealing at different temperatures: 200, 300, 400, and 500 °C.

Figure S4 showed that the $\text{Mn}_1\text{Co}_5\text{O}_x$ treated at 300 °C gave the best OER activity. And the OER activities follow the order of $\text{Mn}_1\text{Co}_5\text{O}_x\text{-}300 > \text{Mn}_1\text{Co}_5\text{O}_x\text{-}200 \approx \text{Mn}_1\text{Co}_5\text{O}_x\text{-}400 > \text{Mn}_1\text{Co}_5\text{O}_x\text{-}500$.

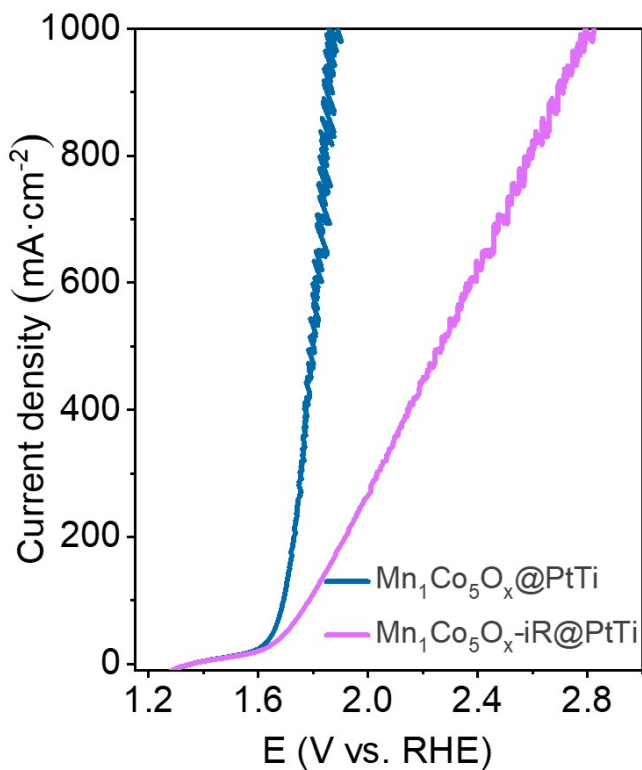


Fig. S7 OER polarization curves of $\text{Mn}_1\text{Co}_5\text{O}_x$ on PtTi mesh in room temperature are in a 0.5 M H_2SO_4 (pH 0) solution.

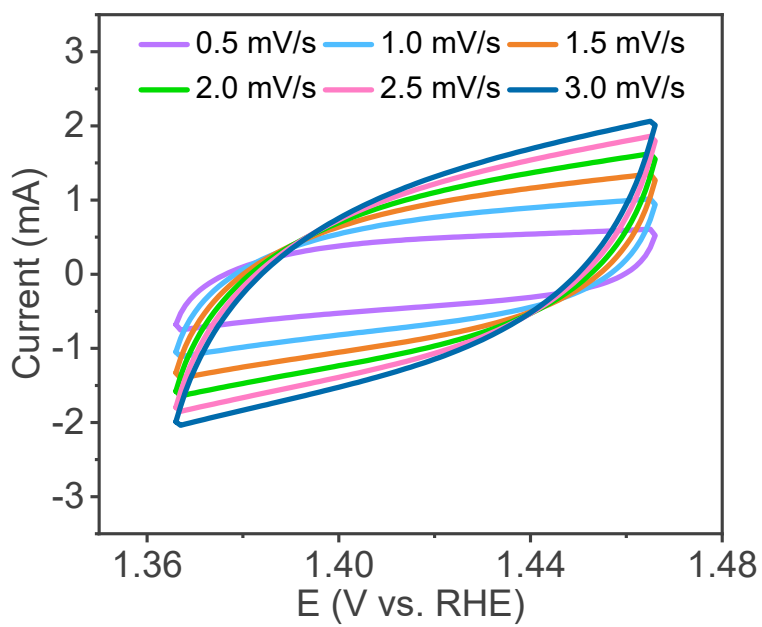


Fig. S8 ECSA measurement of $\text{Mn}_1\text{Co}_5\text{O}_x$. Cyclic voltammograms were measured in a non-Faradaic region of the voltammogram at the following scan rate: 0.5, 1.0, 1.5, 2.0, 2.5, and 3.0 mV/s. All currents were assumed to be due to capacitive charging.

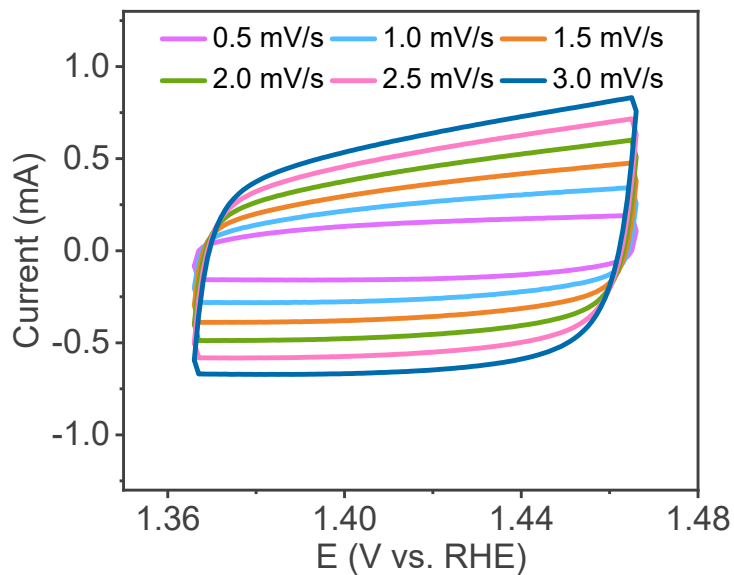


Fig. S9 ECSA measurement of Co_3O_4 . Cyclic voltammograms were measured in a non-Faradaic region of the voltammogram at the following scan rate: 0.5, 1.0, 1.5, 2.0, 2.5, and 3.0 mV/s. All currents were assumed to be due to capacitive charging.

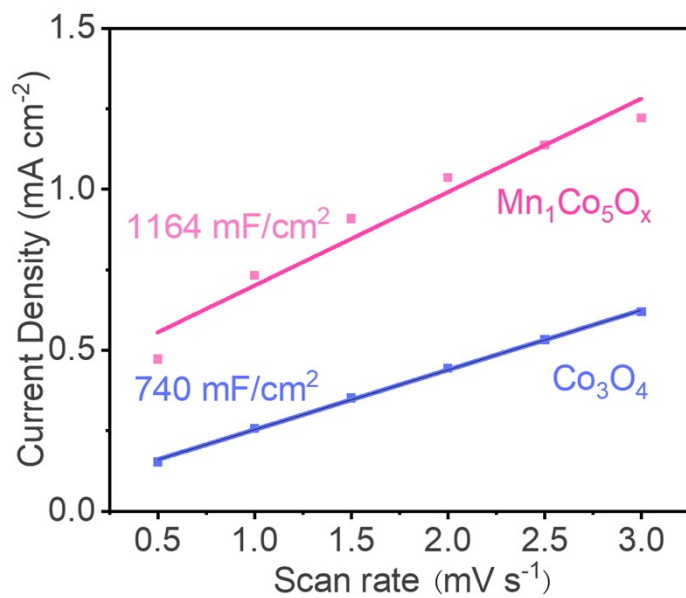


Fig. S10 C_{dl} values of $\text{Mn}_1\text{Co}_5\text{O}_x$ and Co_3O_4 .

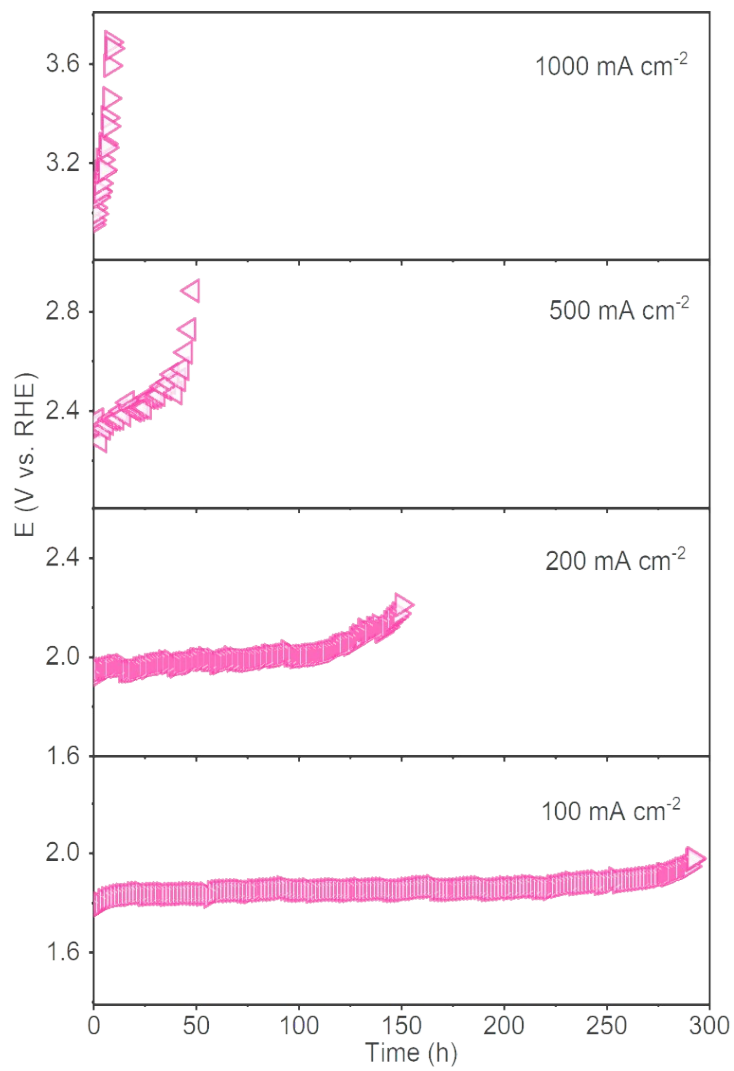


Fig. S11 Chronopotentiometric measurement of the $\text{Mn}_1\text{Co}_5\text{O}_x$ catalyst under current density of 100 , 200 , 500 and 1000 mA cm^{-2} in $0.5 \text{ M H}_2\text{SO}_4$.

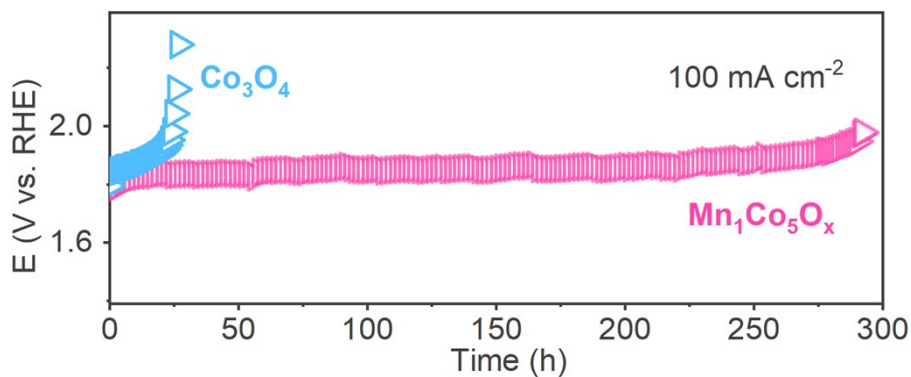


Fig. S12 Chronopotentiometric measurement of the $\text{Mn}_1\text{Co}_5\text{O}_x$ and Co_3O_4 at 100 mA cm^{-2} in a $0.5 \text{ M H}_2\text{SO}_4$ (pH 0) solution at room temperature.

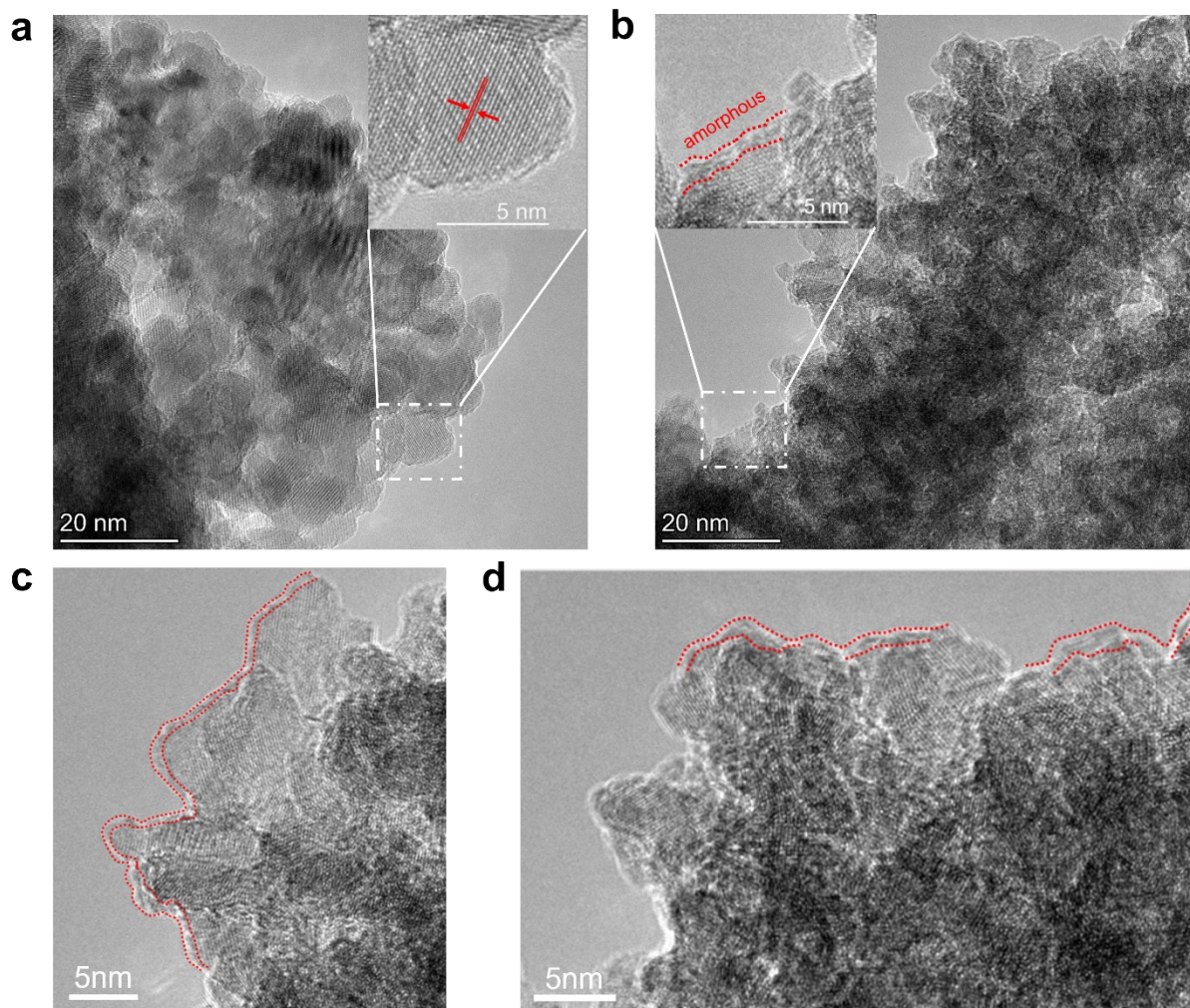


Fig. S13 Comparison of the TEM images of (a) pristine and (b-d) utilized $\text{Mn}_1\text{Co}_5\text{O}_x$ catalysts.

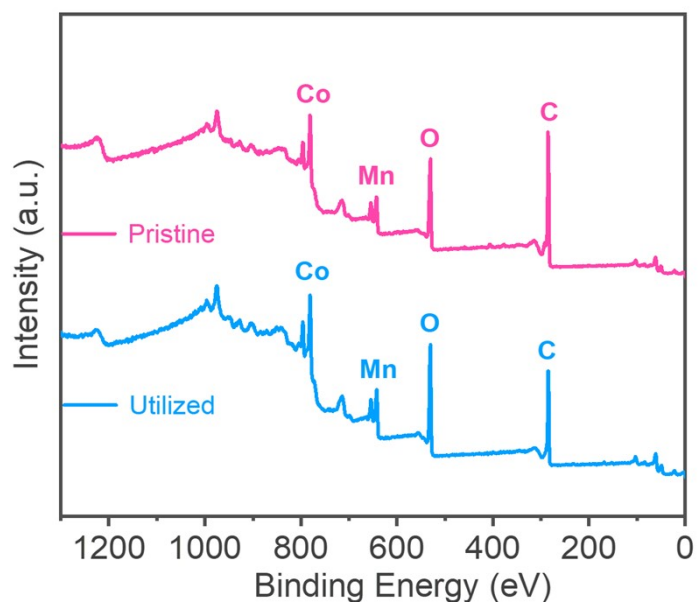


Fig. S14 Full range XPS survey spectra of the pristine and utilized $\text{Mn}_1\text{Co}_5\text{O}_x$ catalysts.

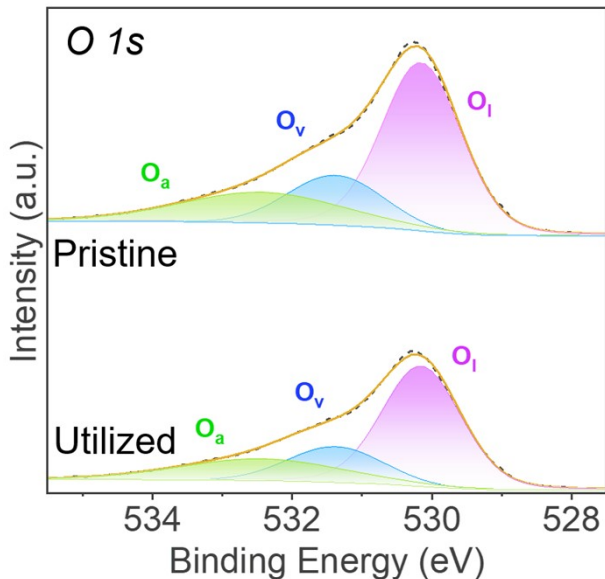


Fig. S15 O 1s XPS spectra of the pristine and utilized $\text{Mn}_1\text{Co}_5\text{O}_x$ catalysts.

Interestingly, the oxidation states of both cobalt and manganese were largely reduced after the OER electrolysis. Also, the population of oxygen vacancy (O_v) decreased. The appearance of hydroxyl groups (O_a , at 533.1 eV) in the utilized $\text{Mn}_1\text{Co}_5\text{O}_x$ catalyst, demonstrated the surface amorphous structure of the utilized oxide electrocatalyst and is well consistent with the observation in its TEM image (Figure S11b).

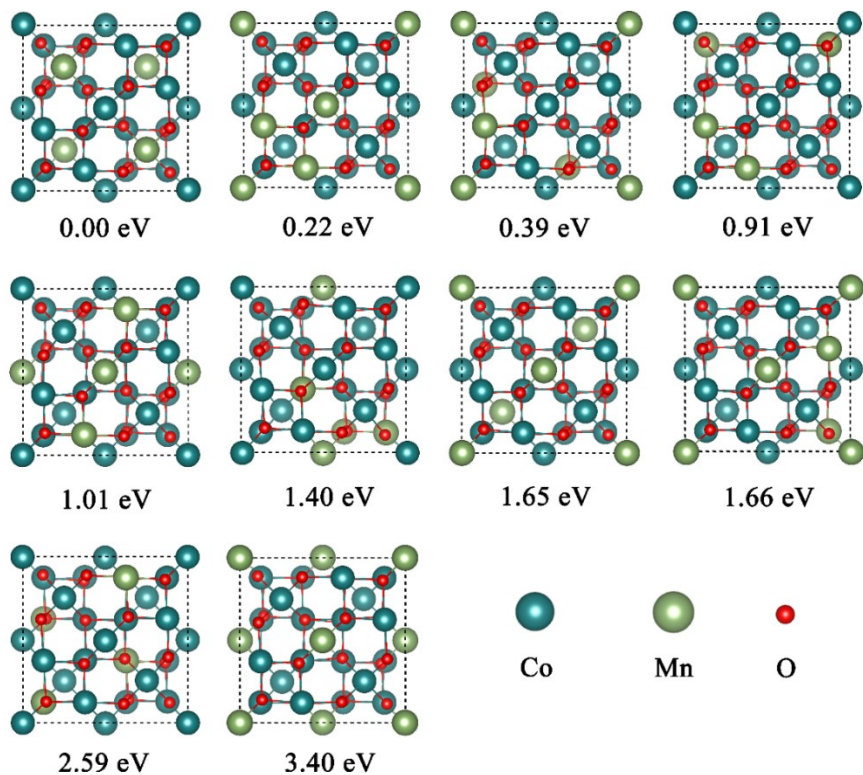


Fig. S16 The configurations and relative energies of the $\text{Mn}_1\text{Co}_5\text{O}_x$ systems.

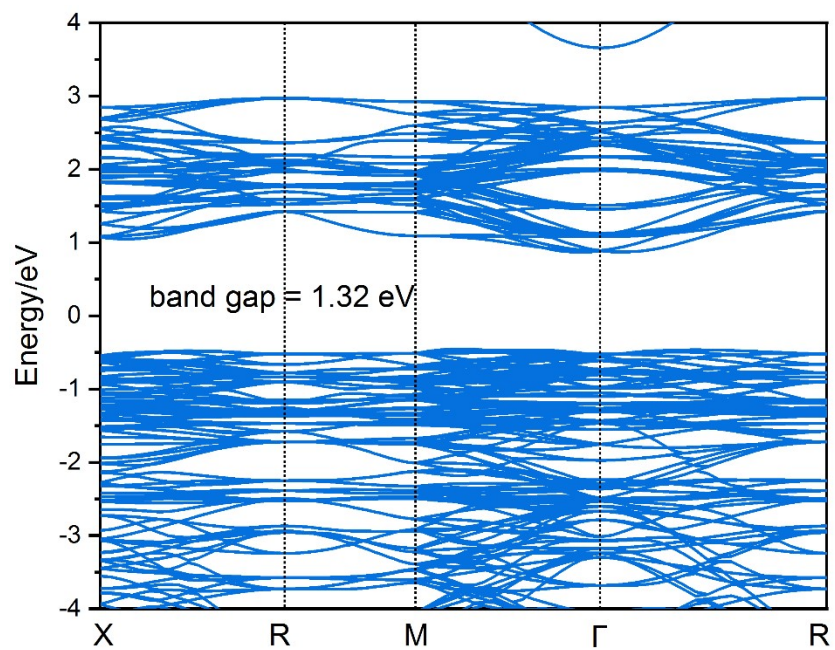


Fig. S17 The band structure of Co_3O_4 bulk structure.

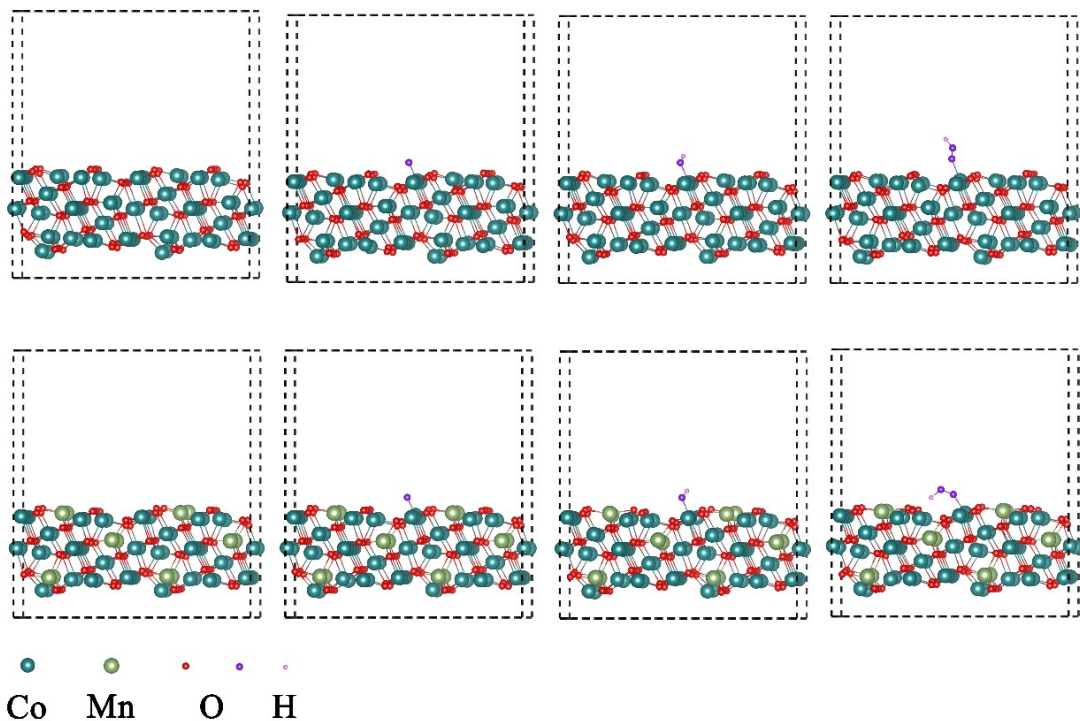


Fig. S18 The configurations of OER reaction coordinates.

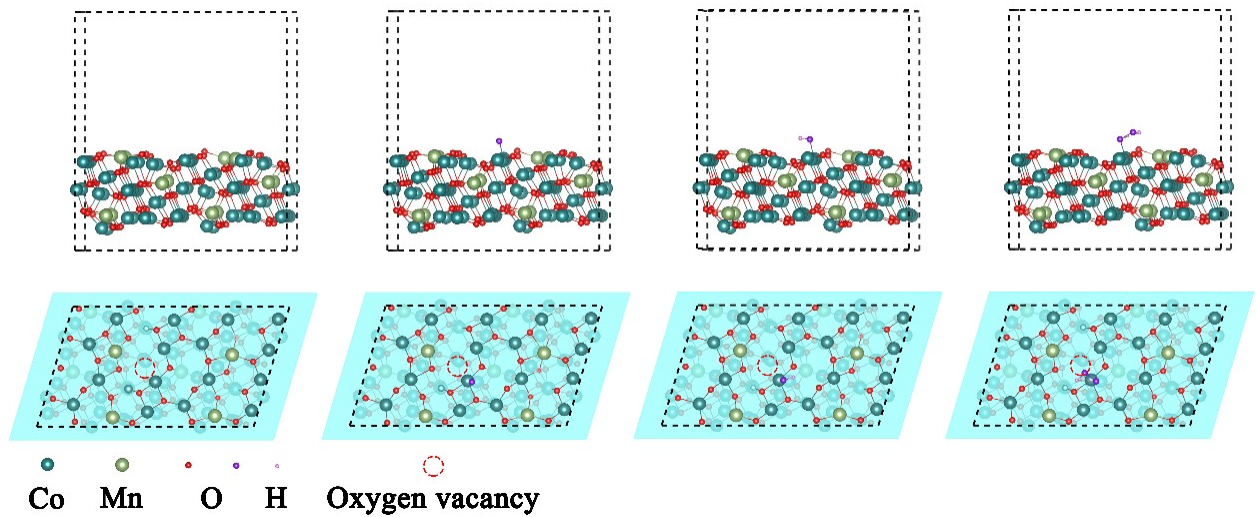


Fig. S19 Configuration of OER reaction coordinates on the Mn-doped Co_3O_4 (311) surface with oxygen vacancy.

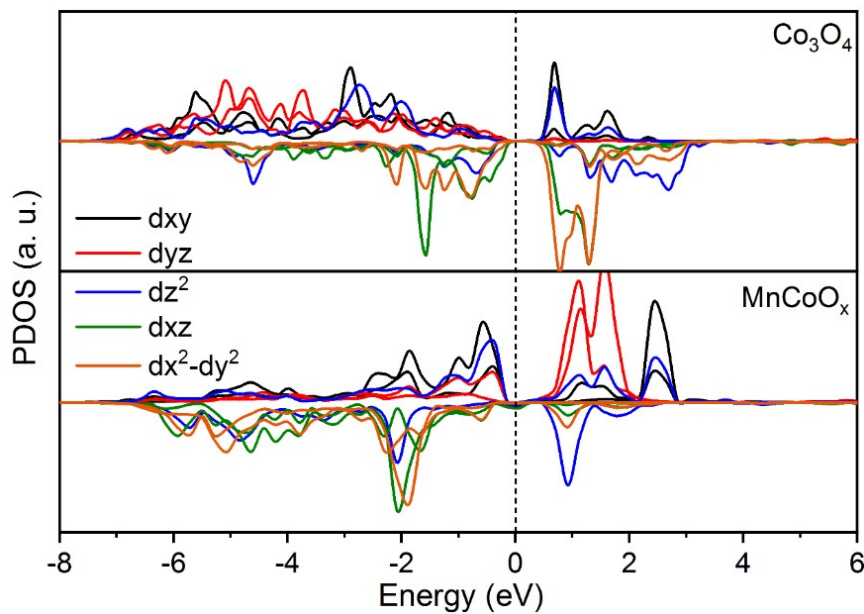


Fig. S20 The project density of states of d orbital.

The introduction of Mn results in a slight protrusion near the Fermi level. This leads to an increase in the number of electrons, possibly indicating some electronic activity of the system in the Oxygen Evolution Reaction (OER). Furthermore, different d -orbitals may play distinct roles in various steps of the OER. The dx^2-y^2 orbital may play a critical role in oxygen decomposition, due to the introduction of Mn, the dx^2-y^2 orbital exhibits higher occupancy below the Fermi level. This typically suggests that the MnCoO_x has more d -electrons available for participation in the OER.

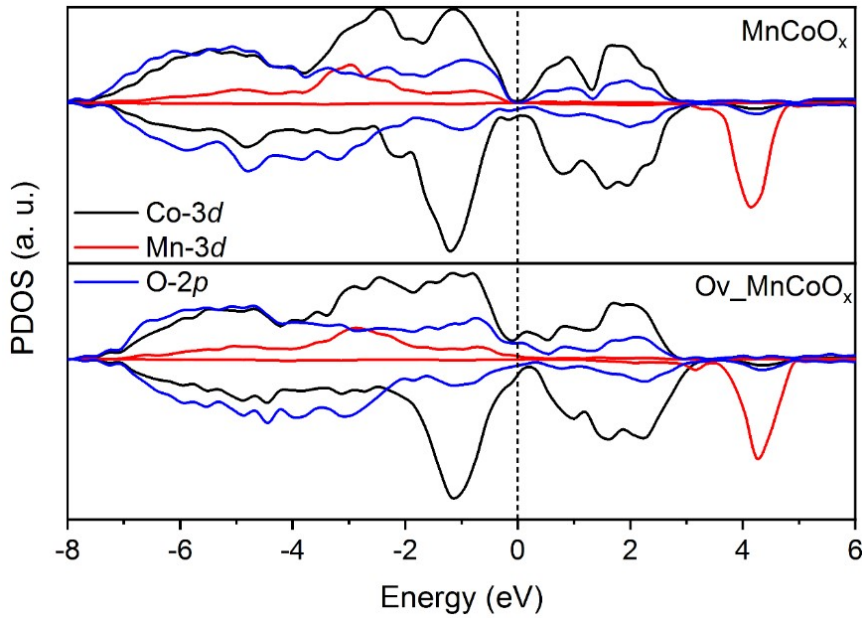


Fig. S21 The project density of states of MnCoO_x and $\text{Ov}_\text{-}\text{MnCoO}_x$.

There is a sharp increase near the Fermi level, indicating an enhancement in the electrical conductivity of system, facilitating the flow of electrons, thereby promoting electron participation in the Oxygen Evolution Reaction (OER).

Supporting Tables

Table S1. XPS analysis of MnCoO_x samples.

Sample	$\text{Co}^{3+}\%$	$\text{Co}^{2+}\%$	$\text{Mn}^{4+}\%$	$\text{Mn}^{3+}\%$	$\text{O}_1\%$	$\text{O}_v\%$	$\text{O}_a\%$	$\text{Co}^{3+}/\text{Co}^{2+}$	$\text{Mn}^{4+}/\text{Mn}^{3+}$
$\text{Mn}_1\text{Co}_{1.5}\text{O}_x$	67.0	33.0	44.1	55.9	54.2	24.0	21.8	2.0	0.8
$\text{Mn}_1\text{Co}_{2.5}\text{O}_x$	65.1	34.9	46.3	53.7	59.1	27.5	13.4	1.9	0.9
$\text{Mn}_1\text{Co}_5\text{O}_x$ -pristine	57.3	42.7	49.3	50.7	54.4	32.6	13.0	1.3	1.0
$\text{Mn}_1\text{Co}_8\text{O}_x$	49.7	50.3	46.6	53.4	64.1	20.9	15.0	1.0	0.9
$\text{Mn}_1\text{Co}_5\text{O}_x$ -utilized	45.9	54.1	38.8	61.2	58.8	19.4	21.8	0.9	0.6
Co_3O_4	35.0	65.0	0	0	66.5	26.5	7.0	0.5	0

The fitted ratios of $\text{Co}^{3+}/\text{Co}^{2+}$ and $\text{Mn}^{4+}/\text{Mn}^{3+}$ in pristine $\text{Mn}_1\text{Co}_5\text{O}_x$ catalyst is much higher than the utilized catalyst, which indicates both the Co^{3+} and Mn^{4+} species were reduced during the OER test. Meanwhile, the population of oxygen vacancy (O_v) also was decreased.

Table S2. Summary of the OER performance in acidic electrolytes for water splitting.

Catalyst	Electrolyte	Performance	Stability	Ref.
Co ₃ O ₄ /FTO	0.5 M H ₂ SO ₄	570 mV@10 mA cm ⁻²	12 h@10 mA cm ⁻²	[1]
Co-Fe Prussian blue	pH 2.0 with Pi	690 mV@10 mA cm ⁻²	6 h@10 mA cm ⁻²	[2]
amorphous CoMnO _x	pH 2.0 in Pi	770 mV@10 mA cm ⁻²	50 h@1 mA cm ⁻² geo	
amorphous CoFePbO _x	pH 2.0 in Pi	770 mV@10 mA cm ⁻²	50 h@1 mA cm ⁻² geo	
amorphous CoPbO _x	pH 2.5 in Pi	620 mV@10 mA cm ⁻²	<8 h@1 mA cm ⁻² geo	[3]
amorphous CoFeO _x	pH 2.0 in Pi	620 mV@10 mA cm ⁻²	<2 h@1 mA cm ⁻² geo	
Co ₃ O ₄ @C	0.5 M H ₂ SO ₄	370 mV@10 mA cm ⁻²	86.8 h@100 mA cm ⁻²	[4]
Co ₂ TiO ₄	0.5 M H ₂ SO ₄	513 mV@10 mA cm ⁻²	~5 h@~10 mA cm ⁻²	[5]
Co-doped 6H-SrIrO ₃	0.1 M HClO ₄	235 mV@10 mA cm ⁻²	20 h@10 mA cm ⁻²	[6]
Mn-RuO ₂	0.5 M H ₂ SO ₄	158 mV@10 mA cm ⁻²	~3 h@~10 mA cm ⁻²	[7]
Ru-MnO ₂	0.1 M HClO ₄	161 mV@10 mA cm ⁻²	200 h@10 mA cm ⁻²	[8]
Co ₂ MnO ₄	0.05 M H ₂ SO ₄	395 mV@10 mA cm ⁻²	320 h@100 mA cm ⁻²	[9]
Co-RuIr	0.1 M HClO ₄	235 mV@10 mA cm ⁻²	25 h@10 mA cm ⁻²	[10]
W-Ir-B	0.5 M H ₂ SO ₄	497 mV@2000 mA cm ⁻²	800 h@100 mA cm ⁻²	[11]
H-Ti@IrO ₂	0.5 M H ₂ SO ₄	336 mV@200 mA cm ⁻²	130 h@200 mA cm ⁻²	[12]
Co _{0.05} Fe _{0.95} O _y	pH 0.3 H ₂ SO ₄	650 mV@10 mA cm ⁻²	50 h@10 mA cm ⁻²	[13]
MnMoCoO _x	2 M H ₂ SO ₄	305 mV@100 mA cm ⁻²	~1 h@~65 mA cm ⁻²	[14]
CoFePbO _x	0.5 M H ₂ SO ₄	700 mV@10 mA cm ⁻² 700 mV@500 mA cm ⁻²	14 h@10 mA cm ⁻² 7 h@500 mA cm ⁻²	[15]
Mn _x Sb _{1-x} O _z	1 M H ₂ SO ₄	580 mV@50 mA cm ⁻²	2 h@10 mA cm ⁻²	[16]
Cu _{1.5} Mn _{1.5} O ₄ -200	0.5 M H ₂ SO ₄	324 mV@10 mA cm ⁻²	20 h@10 to 1.5 mA cm ⁻²	
Cu _{1.5} Mn _{1.5} O ₄ -800	0.5 M H ₂ SO ₄	352 mV@10 mA cm ⁻²	20 h@3.2 to 2.8 mA cm ⁻²	[17]
amorphous Ti:MnO ₂	0.5 M H ₂ SO ₄	670 mV@10 mA cm ⁻²	2 h@7.2 to 6 mA cm ⁻²	[18]
Ni ₂ Ta	0.5 M H ₂ SO ₄	570 mV@10 mA cm ⁻²	66 h@10 mA cm ⁻²	[19]
NiFeP	0.05 M H ₂ SO ₄	540 mV@10 mA cm ⁻²	30 h@10 mA cm ⁻²	[20]
F-doped Cu _{1.5} Mn _{1.5} O ₄	pH 0.3 H ₂ SO ₄	320 mV@10 mA cm ⁻²	24 h@16 mA cm ⁻²	[21]
Ir-Co ₃ O ₄	0.5 M H ₂ SO ₄	236 mV@10 mA cm ⁻²	30 h@10 mA cm ⁻²	[22]
RuO ₂ /(Co,Mn) ₃ O ₄	0.5 M H ₂ SO ₄	270 mV@10 mA cm ⁻²	24 h@10 mA cm ⁻²	[23]

RuIr@CoNC	0.5 M H ₂ SO ₄	223 mV@10 mA cm ⁻²	40 h@10 mA cm ⁻²	[24]
Ni-RuO ₂	0.1 M HClO ₄	214 mV@10 mA cm ⁻²	200 h@10 mA cm ⁻²	[25]
Mn-doped Ru /RuO ₂ @CNT	0.5 M H ₂ SO ₄	177 mV@10 mA cm ⁻²	100 h@100 mA cm ⁻²	[26]
Nd _{0.1} RuO _x	0.5 M H ₂ SO ₄	211 mV@10 mA cm ⁻²	50 h@10 mA cm ⁻²	[27]
Ru ₁ -Pt ₃ Cu	0.1 M HClO ₄	220 mV@10 mA cm ⁻²	28 h@10 mA cm ⁻²	[28]
Cr _{0.6} Ru _{0.4} O ₂	0.5 M H ₂ SO ₄	178 mV@10 mA cm ⁻²	10 h@10 mA cm ⁻²	[29]
Y _{1.7} Sr _{0.3} Ru ₂ O ₇	0.5 M H ₂ SO ₄	264 mV@10 mA cm ⁻²	28 h@10 mA cm ⁻²	[30]
IrRu@Te	0.5 M H ₂ SO ₄	220 mV@10 mA cm ⁻²	20 h@10 mA cm ⁻²	[31]
RuIr-NC	0.05 M H ₂ SO ₄	165 mV@10 mA cm ⁻²	120 h@10 mA cm ⁻²	[32]
IrCo@IrO _x -nL NDs	0.05 M H ₂ SO ₄	247 mV@10 mA cm ⁻²	10 h@2.5 mA cm ⁻²	[33]
W _{0.2} Er _{0.1} Ru _{0.7} O _{2-δ}	0.5 M H ₂ SO ₄	168 mV@10 mA cm ⁻²	120 h@100 mA cm ⁻²	[34]
IrO _x /9R-BaIrO ₃	0.5 M H ₂ SO ₄	230 mV@10 mA cm ⁻²	40 h@10 mA cm ⁻²	[35]
MnCo ₅ O _x solid solution	0.5 M H ₂ SO ₄	275 mV@10 mA cm ⁻² 569 mV@100 mA cm ⁻² (non - IR compensation)	300 h@100 mA cm ⁻²	This work

Table S3. The ICP results of electrolyte for stability testing at 100 mA cm⁻² of Co₃O₄ and Mn₁Co₅O_x.

Samples	Stability testing time (h)	The electrolyte's Mn concentration (ppm)	The electrolyte's Co concentration (ppm)
Co ₃ O ₄	14	-0.25	89.43
Mn ₁ Co ₅ O _x	25	6.01	37.95

References

- 1 J. S. Mondschein, J. F. Callejas, C. G. Read, J. Y. C. Chen, C. F. Holder, C. K. Badding and R. E. Schaak, *Chem. Mater.*, 2017, **29**, 950-957.
- 2 L. Han, P. Tang, Á. Reyes-Carmona, B. Rodríguez-García, M. Torréns, J. R. Morante, J. Arbiol and J. R. Galan-Mascaros, *J. Am. Chem. Soc.*, 2016, **138**, 16037-16045.
- 3 M. Huynh, T. Ozel, C. Liu, E. C. Lau and D. G. Nocera, *Chem. Sci.*, 2017, **8**, 4779-4794.
- 4 X. Yang, H. Li, A.-Y. Lu, S. Min, Z. Idriss, M. N. Hedhili, K.-W. Huang, H. Idriss and L.-J. Li, *Nano Energy*, 2016, **25**, 42-50.
- 5 S. Anantharaj, K. Karthick and S. Kundu, *Inorg. Chem.*, 2019, **58**, 8570-8576.
- 6 L. Yang, H. Chen, L. Shi, X. Li, X. Chu, W. Chen, N. Li and X. Zou, *ACS Appl. Mater. Interfaces*, 2019, **11**, 42006-42013.
- 7 S. Chen, H. Huang, P. Jiang, K. Yang, J. Diao, S. Gong, S. Liu, M. Huang, H. Wang and Q. Chen, *ACS Catal.*, 2019, **10**, 1152-1160.
- 8 C. Lin, J.-L. Li, X. Li, S. Yang, W. Luo, Y. Zhang, S.-H. Kim, D.-H. Kim, S. S. Shinde, Y.-F. Li, Z.-P. Liu, Z. Jiang and J.-H. Lee, *Nat. Catal.*, 2021, **4**, 1012-1023.
- 9 A. Li, S. Kong, C. Guo, H. Ooka, K. Adachi, D. Hashizume, Q. Jiang, H. Han, J. Xiao and R. Nakamura, *Nat. Catal.*, 2022, **5**, 109-118.
- 10 J. Shan, T. Ling, K. Davey, Y. Zheng and S. Z. Qiao, *Adv. Mater.*, 2019, **31**, 1900510.
- 11 R. Li, H. Wang, F. Hu, K. C. Chan, X. Liu, Z. Lu, J. Wang, Z. Li, L. Zeng, Y. Li, X. Wu and Y. Xiong, *Nat. Commun.*, 2021, **12**, 3540.
- 12 Z. Yu, J. Xu, Y. Li, B. Wei, N. Zhang, Y. Li, O. Bondarchuk, H. Miao, A. Araujo, Z. Wang, J. L. Faria, Y. Liu and L. Liu, *J. Mater. Chem. A*, 2020, **8**, 24743-24751.
- 13 W. L. Kwong, C. C. Lee, A. Shchukarev and J. Messinger, *Chem. Commun.*, 2019, **55**, 5017-5020.
- 14 D. Delgado, M. Minakshi, J. McGinnity and D.-J. Kim, *Sci. Rep.*, 2015, **5**, 15208.
- 15 M. Chatti, J. L. Gardiner, M. Fournier, B. Johannessen, T. Williams, T. R. Gengenbach, N. Pai, C. Nguyen, D. R. MacFarlane, R. K. Hocking and A. N. Simonov, *Nat. Catal.*, 2019, **2**, 457-465.
- 16 L. Zhou, A. Shinde, J. H. Montoya, A. Singh, S. Gul, J. Yano, Y. Ye, E. J. Crumlin, M. H. Richter, J. K. Cooper, H. S. Stein, J. A. Haber, K. A. Persson and J. M. Gregoire, *ACS Catal.*, 2018, **8**, 10938-10948.
- 17 S. D. Ghadge, M. K. Datta, O. I. Velikokhatnyi, R. Kuruba, P. M. Shanthi and P. N. Kumta, *J. Electrochem. Soc.*, 2020, **167**, 144511.

- 18 R. Frydendal, E. A. Paoli, I. Chorkendorff, J. Rossmeisl and I. E. L. Stephens, *Adv. Energy Mater.*, 2015, **5**, 1500991.
- 19 J. S. Mondschein, K. Kumar, C. F. Holder, K. Seth, H. Kim and R. E. Schaak, *Inorg. Chem.*, 2018, **57**, 6010-6015.
- 20 F. Hu, S. Zhu, S. Chen, Y. Li, L. Ma, T. Wu, Y. Zhang, C. Wang, C. Liu, X. Yang, L. Song, X. Yang and Y. Xiong, *Adv. Mater.*, 2017, **29**, 1606570-1606570.
- 21 P. P. Patel, M. K. Datta, O. I. Velikokhatnyi, R. Kuruba, K. Damodaran, P. Jampani, B. Gattu, P. M. Shanthi, S. S. Damle and P. N. Kumta, *Sci. Rep.*, 2016, **6**, 28367.
- 22 Y. Zhu, J. Wang, T. Koketsu, M. Kroschel, J. M. Chen, S. Y. Hsu, G. Henkelman, Z. Hu, P. Strasser and J. Ma, *Nat. Commun.*, 2022, **13**, 7754.
- 23 S. Niu, X.-P. Kong, S. Li, Y. Zhang, J. Wu, W. Zhao and P. Xu, *Appl. Catal. B: Environ.*, 2021, **297**, 120442.
- 24 J. Xu, J. Li, Z. Lian, A. Araujo, Y. Li, B. Wei, Z. Yu, O. Bondarchuk, I. Amorim, V. Tileli, B. Li and L. Liu, *ACS Catal.*, 2021, **11**, 3402-3413.
- 25 Z.-Y. Wu, F.-Y. Chen, B. Li, S.-W. Yu, Y. Z. Finfrock, D. M. Meira, Q.-Q. Yan, P. Zhu, M.-X. Chen, T.-W. Song, Z. Yin, H.-W. Liang, S. Zhang, G. Wang and H. Wang, *Nat. Mater.*, 2023, **22**, 100-108.
- 26 W. Xu, H. Huang, X. Wu, Y. Yuan, Y. Liu, Z. Wang, D. Zhang, Y. Qin, J. Lai and L. Wang, *Compos. Part B: Eng.*, 2022, **242**, 110013.
- 27 L. Li, G. Zhang, J. Xu, H. He, B. Wang, Z. Yang and S. Yang, *Adv. Funct. Mater.*, 2023, **33**, 2213304.
- 28 Y. Yao, S. Hu, W. Chen, Z.-Q. Huang, W. Wei, T. Yao, R. Liu, K. Zang, X. Wang, G. Wu, W. Yuan, T. Yuan, B. Zhu, W. Liu, Z. Li, D. He, Z. Xue, Y. Wang, X. Zheng, J. Dong, C.-R. Chang, Y. Chen, X. Hong, J. Luo, S. Wei, W.-X. Li, P. Strasser, Y. Wu and Y. Li, *Nat. Catal.*, 2019, **2**, 304-313.
- 29 Y. Lin, Z. Tian, L. Zhang, J. Ma, Z. Jiang, B. J. Deibert, R. Ge and L. Chen, *Nat. Commun.*, 2019, **10**, 162.
- 30 N. Zhang, C. Wang, J. Chen, C. Hu, J. Ma, X. Deng, B. Qiu, L. Cai, Y. Xiong and Y. Chai, *ACS Nano*, 2021, **15**, 8537-8548.
- 31 J. Xu, Z. Lian, B. Wei, Y. Li, O. Bondarchuk, N. Zhang, Z. Yu, A. Araujo, I. Amorim, Z. Wang, B. Li and L. Liu, *ACS Catal.*, 2020, **10**, 3571-3579.

- 32 D. Wu, K. Kusada, S. Yoshioka, T. Yamamoto, T. Toriyama, S. Matsumura, Y. Chen, O. Seo, J. Kim, C. Song, S. Hiroi, O. Sakata, T. Ina, S. Kawaguchi, Y. Kubota, H. Kobayashi and H. Kitagawa, *Nat. Commun.*, 2021, **12**, 1145.
- 33 G. Meng, W. Sun, A. A. Mon, X. Wu, L. Xia, A. Han, Y. Wang, Z. Zhuang, J. Liu, D. Wang and Y. Li, *Adv. Mater.*, 2019, **31**, 1903616.
- 34 S. Hao, M. Liu, J. Pan, X. Liu, X. Tan, N. Xu, Y. He, L. Lei and X. Zhang, *Nat. Commun.*, 2020, **11**, 5368.
- 35 N. Li, L. Cai, C. Wang, Y. Lin, J. Huang, H. Sheng, H. Pan, W. Zhang, Q. Ji, H. Duan, W. Hu, W. Zhang, F. Hu, H. Tan, Z. Sun, B. Song, S. Jin and W. Yan, *J. Am. Chem. Soc.*, 2021, **143**, 18001-18009.